# Revisiting cathode-electrolyte interfaces in batteries

Jie Xiao[*1,2], Nicole Adelstein[3], Yujing Bi[1], Wenjuan Bian[4], Jordi Cabana[5], Corie L. Cobb[2], Yi Cui[6,7], Shen J. Dillon[8], Marca M. Doeff[9], Saiful M. Islam[10], Kevin Leung[11], Mengya Li[12], Feng Lin[13], Jun Liu[1,2], Hongmei Luo[14], Amy C. Marschilok[15,16], Ying Shirley Meng[17], Yue Qi[18], Ritu Sahore[12], Kayla G. Sprenger[19], Robert C. Tenent[20], Michael F. Toney[19], Wei Tong[8], Liwen F. Wan[21], Chongmin Wang[1], Stephen E. Weitzner[21], Bingbin Wu[1], Yaobin Xu[1]

[1]Pacific Northwest National Laboratory, Richland, WA, United States
[2]University of Washington, Seattle, WA, United States
[3]San Francisco State University, San Francisco, CA, United States
[4]Idaho National laboratory, Idaho Falls, ID, United States
[5]Argonne National Laboratory, Lemont, IL, United States
[6]SLAC National Accelerator Laboratory, Menlo Park, CA, United States
[7]Stanford University, Stanford, CA, United States
[8]University of California Irvine, Irvine, CA, United States
[9]Lawrence Berkeley National Laboratory, Berkeley, CA, United States
[10]Jackson State University, Jackson, MS, United States
[11]Sandia National Laboratories, Albuquerque, NM, United States
[12]Oak Ridge National Laboratory, Oak Ridge, TN, United States
[13]Virginia Tech, Blacksburg, VA, United States
[14]New Mexico State University, Las Cruces, NM, United States
[15]Brookhaven National Laboratory, Upton, NY, United States
[16]Stony Brook University, Stony Brook, NY, United States
[17]University of Chicago, Chicago, IL, United States
[18]Brown University, Providence, RI, United States
[19]University of Colorado Boulder, Boulder, CO, United States
[20]National Renewable Energy Laboratory, Golden, CO, United States
[21]Lawrence Livermore National Laboratory, Livermore, CA, United States

Corresponding author. Email: jie.xiao@pnnl.gov



Pursuant to the DOE Public Access Plan, this document represents the authors' peer-reviewed, accepted manuscript. The published version of the article is available from the relevant publisher.

**Abstract**

The Cathode Electrolyte Interface (CEI) plays a pivotal role in determining the usable capacity and cycling stability of electrochemical cells, yet it is overshadowed by its counterpart, the Solid Electrolyte Interface (SEI). This is primarily due to the prevalence of side reactions, particularly at low potentials on the negative electrode, especially in state-of-the-art Li-ion batteries where the charge cutoff voltage is limited. However, as the quest for high-energy battery technologies for electric vehicles intensifies, there is a pressing need to re-examine CEI properties. Here, we present a comprehensive approach to revisiting CEI in battery systems. We underscore the importance of employing model cathode materials and coin cell protocols to establish baseline performances. Additionally, we delve into the reasons behind the inconsistent and occasionally controversial findings on CEI, while also addressing the challenges and opportunities in characterizing and simulating CEI, offering potential solutions to enhance its relevance to real-world devices.



Pursuant to the DOE Public Access Plan, this document represents the authors' peer-reviewed, accepted manuscript.
The published version of the article is available from the relevant publisher.

Almost all electrode couples in electrochemical cells operate beyond the thermodynamic stability limits of electrolytes[1]. In many cases, these cells are only able to operate because the reactions between the electrode and electrolyte form new phases (or interphases) at the electrode–electrolyte interface. The canonical example of this is the stable solid-electrolyte interphase (SEI) layer[2] formed on graphite anode surfaces that enabled the commercialization of Li-ion batteries. Although high-quality SEIs and cathode-electrolyte interphase (CEI) layers may share similarities in terms of their stability, structural density, low impedance, thickness, etc., in practice, the desired attributes of CEI layers are highly battery system- and cathode chemistry-dependent. Unfortunately, there is no universal CEI (or SEI) that can meet the performance demands across all applications. For example, a thin CEI layer is usually preferred for fast ion diffusion[3-5], whereas a denser CEI can help mitigate transition metal dissolution from cathode surfaces[6,7]. Moreover, the ability to form a stable CEI at a high cutoff voltage, e.g., beyond 4.3 V (vs. $Li/Li^+$), is essential for extracting more energy from the conventional layered cathode materials.

Despite the abovementioned significance, the CEI has not attracted as much attention as its SEI counterpart. The main reason for this is likely that for batteries with cutoff voltages below 4.2 V, most carbonate-based electrolytes are stable on the cathode but decompose more aggressively at the anode due to the very low electrode potentials. Nevertheless, as the demand for high energy batteries continues to grow, in addition to the exploration of new high energy materials[8,9], it is important to increase the battery operation voltage appropriately, so more capacity and energy can be extracted from the same set of cathode materials in the cell and pack, assuming their structure remains stable. At elevated voltages, a stable CEI layer becomes critical for both battery performance and the structural stability of the cathode itself. Similar to the SEI, the CEI is generated through the decomposition of electrolytes, albeit at high voltages, creating a passive film on the cathode surface[10]. The presence and nature of the CEI thus directly determines the reversibility and efficiency of ion transport, assuming that the SEI or the anode itself are not hindering the overall cell reactions and acting as key limiting factors. In addition to electrolyte recipes, cathode surface chemistry[11], morphologies[12], and electrode potential[13] all profoundly impact CEI components and properties.

Although there are already many publications focusing on the CEI, a clear consensus has yet to emerge, and a lack of understanding persists on how to design and control CEI layers at the molecular level. Some of the potential reasons behind the inconsistent and sometimes controversial discoveries on CEI include but are not limited to:

(1) **Lack of model materials with controllable surface properties:** Many cathode materials used for CEI studies are synthesized in different labs, leading to variations in particle sizes, morphologies, and even stoichiometry of the as-prepared materials[14,15]. The higher surface area of smaller cathode particles intensifies side reactions and impacts CEI formation[16-18]. Even when commercially sourced cathode materials (e.g., $LiNi_xMn_yCo_zO_2$ (NMC811; x=0.8, y=0.1, z=0.1 in weight percentage)) are used, depending on the storage conditions, the surface chemistry of NMC811 changes significantly, such as when exposed to air[19]. The drastically different surface and bulk properties of cathode materials often determine the observed electrochemical performances, making it hard to isolate the CEI's effect in the electrochemical cell.

(2) **Reliable design of electrochemical cells for operando characterization of CEI:** Electrochemical cells designed for in situ characterization sometimes introduce a significant



Pursuant to the DOE Public Access Plan, this document represents the authors' peer-reviewed, accepted manuscript. The published version of the article is available from the relevant publisher.

increase in cell impedance because of their drastically modified cell format[20]. It is not uncommon that the applied potential is far beyond that normally used to charge small cells. In miniaturized characterization cells, the increased physical distance between cathode and anode is another contributor to the high impedance, particularly when a non-aqueous electrolyte is used. The physics of the operando experiments can require compromising cell architecture to a point where it becomes irrelevant to real-world operation conditions. For example, some synchrotron and transmission electron microscopy (TEM) techniques require high vacuum, meaning non-volatile electrolytes and open cell design must be used. However, in reality the cathode surface is buried deeply inside an operating cell and thus the design of in situ electrochemical cells that approach the behavior of cells designed for battery benchmarking is critical in determining if an observation is a common phenomenon in CEI or only exists in the specific conditions imposed by the operando experiment due to the idiosyncrasies of the design of such small-scale cells[20,21].

(3) **CEI derived from flooded electrolytes vs. CEI formed in lean electrolytes:** Most characterizations are conducted on materials in cells flooded with electrolyte, often at volumes one order of magnitude more than what is practically used in real batteries[22]. The significantly higher amount of electrolyte in flooded cells facilitates CEI dissolution and reformation during cycling. Thus, CEI composition and thickness continuously change. These changes make the observed properties of the CEI poorly representative when it comes to real batteries, in which the CEI is derived from very lean electrolyte conditions.

(4) **Cell failure is NOT dominantly caused by the CEI if the cathode is coupled with a poor anode:** The electrochemical performance of a cell is determined by the worst electrode including its interphase, assuming separators and electrolyte are reasonably good and not the limiting step via impeded $Li^+$ transport. For the initial assessment of CEI, half cells using lithium (Li) metal as the counter electrode will provide useful information, especially in the early stage of electrochemical reactions. Upon cycling, however, the Li metal anode itself becomes unstable due to the formation of mossy/dendritic Li. Cell impedance increases drastically and dominates the instability of performance. To fully understand the CEI and its evolution, especially after extensive cycling, a stable anode and its SEI are prerequisites. Full cells using stable graphite (and stable SEI) as the anode are necessary to ensure that the electrochemical reaction is mainly controlled by the CEI during extensive cycling, thereby enabling an accurate interpretation of the electrochemical data.

A full understanding of CEI formation and evolution at varied length and time scales, especially at high voltages, is still lacking in the battery community. Progress is urgently needed to better tune CEI properties at the atomic scale to further stabilize the electrochemical energy storage system.

## Revisiting CEI at relevant scales

**Full coin cell protocols to ensure CEI dictates the macroscopic performance:** One prerequisite to understand and address CEI challenges at high voltages is to ensure that the interfacial phenomena captured between cathode and electrolyte not only occur in practical batteries, but also play a dominate role in the electrochemical performance. This is because the performance of any electrochemical cell is dictated by the slowest step or worst component during battery operation[23]. If the observed electrochemical performance is not dominated by the CEI, it is challenging to



Pursuant to the DOE Public Access Plan, this document represents the authors' peer-reviewed, accepted manuscript. The published version of the article is available from the relevant publisher.

assess the utility of CEI engineering efforts, since the impact of CEI properties on cell performance is masked by extraneous limiting factors.

Similarly, a stable anode such as graphite is necessary to effectively evaluate CEI and cathode behaviors. If Li metal is used as the counter electrode, there are always excessive amounts of $Li^+$ in the cell. However, in cells with graphite anodes, the Li inventory is restricted to that provided by the cathode. Therefore, the usable capacity of the cathode can be fully realized during the initial cycling, which is helpful for understanding its material properties. Nevertheless, coin cells using Li metal anodes help to design a balanced full cell with appropriate negative/positive (N/P) ratios and have the added benefit of being simpler to assemble. The latter is highly useful for characterization purposes, especially in situ or operando probing. Moreover, for small cycle numbers, the CEI of such half cells will not differ considerably from those in graphite-based full coin cells; however, their long-time cycling behavior will mainly reflect Li metal problems instead of cathode/CEI stability[22]. Thus, it is when the long-term stability of CEI becomes the focus of study that coupling with a stable graphite anode is necessary to ensure the sensitivity of the cell performance to the CEI is properly established.

While preferable for long-term CEI evaluation, graphite-based full cells, in contrast to Li metal half cells, have more parameters to control for to ensure reproducibility, from electrode coating to cell assembly and testing[24]. Table 1 lists the necessary parameters to construct and test full coin cells under conditions that are relevant to practical batteries, while being suitable to evaluate the impact of CEI engineering solutions. A more detailed assembly process can be found in our previously published paper[24]. Depending on the intended application, the areal loading and porosity of cathode (and anode) in Table 1 can be further tuned for high energy, high power, or fast charging systems.

As mentioned earlier, another issue with using a coin cell as the testing vehicle is that the electrolyte, which must fill in all the void spaces in the device, is in large excess compared to that in pouch cells. This fact adds some uncertainty to the study of the CEI dissolution in coin cells, given the flooding by the electrolyte. Therefore, ultimately, a pouch cell with targeted capacity, energy, or power is the best platform for cross-validation. Because they are simpler to assemble, the full coin cell protocol listed in Table 1 should be viewed as a powerful vehicle to quickly identify the most valuable approaches, ensure fair and consistent comparisons, and provide a gateway for further implementation of new materials in full format pouch cells.

## Model cathode materials to investigate CEI at high voltages

Cathode stability at high voltages is impacted by both the interfacial and bulk properties of the material. Therefore, a model cathode material that does not undergo significant structural change at high voltages will be critical to explore CEI formation and evolution. Single crystal nickel (Ni)-rich NMC is a good model material for this purpose. For example, single crystal Ni-rich NMC prepared using a molten salt approach[13] (Figs.1a-c) has controlled morphologies that can be used for various purposes. Cylinder-shaped (Fig. 1a) or drum-like NMC76 (x=0.76, y=0.14, z=0.1) (Fig. 1b) single crystals expose different facets to the liquid electrolyte, providing a unique opportunity to study prepared CEI formation or decomposition, if any, on specific lattice planes. Single crystals of NMC76 can also grow as large as ~30 μm in diameter (Fig. 1c) and still display electrochemical activity, albeit at a very slow rate (Fig. 1g), rendering them a perfect platform for operando



Pursuant to the DOE Public Access Plan, this document represents the authors' peer-reviewed, accepted manuscript.
The published version of the article is available from the relevant publisher.

characterization of CEI in a "living" electrochemical cell. Irregularly shaped NMC811 single crystals (Fig. 1d) developed from solid state synthesis[25] provide a good comparison to those formed on crystals grown from molten salts, as the surface properties and impurity levels are quite different from the beginning of processing. For each model cathode, a baseline performance derived from full coin cells using the corresponding protocols will be critical to benchmark future results.

Commercial polycrystalline NMC811 are also good model materials to establish convincing baseline performance compared to lab-made cathode materials, using similar cell parameters and testing conditions. Unfortunately, it is not uncommon in the literature to use poorly performing and poorly characterized cathodes as controls to misleadingly claim an improvement of modified materials, which is detrimental to advancing technology development. Figure 2 is an example of coin cell performances that can be used as a baseline for NMC (or graphite) research. The NMC811 cathode and graphite anode are both from commercial sources. The electrolyte used is the same baseline electrolyte listed in Table 1. Electrodes are constructed corresponding to the key parameters in Table 1. It is clear that, between 2.6 and 4.2 V, very stable cycling is achievable from Graphite/NMC811 coin cells without modifying electrodes or using any additives. Even when the cutoff voltage is increased to 4.3V (vs. graphite), the full coin cell still demonstrated stable cycling stability with 82.7% capacity retention after 500 cycles, similar to the cells cycled between 2.6 and 4.2V.

In fact, any cathode material can be used as a model material to study the CEI or its own structural stability, provided that the cathode and CEI are the controlling factors determining the cell performance. Upon establishment of baseline performance, CEI improvements achieved via surface coating or electrolyte reformulation will become rational and reproducible. Still for materials exhibiting extraordinary CEI stability at the materials level, implementations at the particle level with high mass loading and controlled porosity remains challenging[26-28].

## Electrolytes and additives for the stabilization of the CEI

**High voltage operation of Li-ion batteries:** To stabilize the CEI at high voltages, it is first necessary to define how high a cutoff must be reached in an EV battery based on Li-ion chemistry. Table 2 compares the gain in capacity and energy and the reduction of a critical element such as cobalt in a 100 kWh EV battery pack adopting Graphite/NMC chemistry charged to various cutoff voltages.

**NMC811:** The cutoff voltage is usually set to 4.2 V (vs. graphite, corresponding to 4.3 V vs. $Li/Li^+$) for commercial Li-ion batteries. If charged to 4.3 V vs. graphite, the usable discharge capacity of NMC811 is increased from 190 mAh/g (at 4.2 V vs. graphite) to 210 mAh/g, accompanied by a slightly increased average discharge voltage. The capacity gain of 20 mAh/g simply by raising the cutoff voltage effectively increases cell level energy and provides more needed flexibility for the cell level design. For the same 100 kWh pack, increasing the cutoff voltage from 4.2 to 4.3V also means less cathode material may be needed to meet an energy target, reducing battery pack weight by 17 kg and the amount of cobalt by 1 kg. Further increasing the cutoff voltage of Gr/NMC811 couple to 4.4 V extracts a slightly higher capacity by 5 mAh/g, but the advantages become limited (Table 2). It is probably not worthwhile to increase the upper limit by 100 mV because of the very strict requirements needed for solvent purity and anodic stability.



Pursuant to the DOE Public Access Plan, this document represents the authors' peer-reviewed, accepted manuscript.
The published version of the article is available from the relevant publisher.

Usually, the entire electrochemical stability window of the electrolyte shifts towards either higher or lower potentials in the same direction. Expanding the window towards both high and low voltage ranges simultaneously is quite challenging. Consequently, the electrolyte that stabilizes the CEI at very high voltages beyond 4.3 V could easily become unstable with respect to the anode. Additionally, Ni-rich NMCs are not stable beyond 4.3 V (vs. graphite) due to phase transitions and increased probability of gas evolution. Therefore, developing a functional electrolyte that ensures a stable CEI above 4.3 V (vs. graphite) may not be useful, unless the structural instability of NMC811 itself is addressed first.

**Beyond NMC811:** NMC with very high Ni content, e.g., NMC95 (x=0.95, y=0.04, z=0.01) is only stable to 4.04 V vs. graphite[29]. Aggressive side reactions occur between the cathode surface and the electrolyte even at 4.18 V (vs. graphite), which is reflected by the continuous cathode impedance growth upon cycling. Therefore, the definition of "high" voltage depends on cathode composition and may differ from that of cells containing NMC811. In this case, stabilizing Ni-rich NMC below 4.3 V (vs. graphite) or 4.4 V (vs. $Li/Li^+$) is sufficient to balance energy gain and cycling stability. For example, for NMC90 (x=0.9, y=0.05, z=0.05), the charge cutoff voltage that enables stable cycling may reside between 4.1 and 4.2 V and requires further study. The amount of cobalt in the same 100 kWh EV pack using NMC90 is reduced to half while providing more energy with less battery weight (Table 2). The problem with NMC90 is that even if the electrochemical window is limited to 2.6-4.2 V (vs. graphite), its stability is already worse than NMC811 cycled within the same voltage range due to the unstable Ni-rich surface and severe growth of impedance upon cycling. This fact makes pushing the cutoff voltage to 4.3 V a daunting endeavor at the current time. Thermal stability is another concern if the Ni content is too high in NMC. Single crystal morphologies may help stabilize NMC811 and NMC90 at elevated potentials, but more work is still needed to confirm this promise. In addition to morphology control, for NMC90 (or compositions with even higher Ni content), stable electrolytes that are resistant to highly active O, suppress cathode impedance growth, and enhance the thermal stability of the cathode need to be identified to unlock their full potential. Optimization of Ni content in NMC with an electrochemical window that matches currently available functional electrolytes may also provide means to balance the energy, cycle life, and safety of Li-ion batteries employing high Ni-content NMCs as cathodes.

## Understanding the CEI in a relevant battery system

The CEI builds from decomposition byproducts of the electrolyte on the cathode particle surfaces. Therefore, the electrolyte constituents and their relative stability during polarization largely determine the CEI components. The effective evaluation of electrolytes and their derived CEI layers is built upon a few assumptions including but not limited to: (1) the cathode itself is free of pre-existing surface impurities left over from synthesis[30] or developed during storage[19], (2) the electrolyte has no residual water or other impurities that will detrimentally affect the cell performance[31], and (3) no migration of transition metal cations from the cathode to the anode, which may damage the SEI, causing fast cell degradation. All in all, the SEI should always be more stable compared to the CEI. Some of the modified electrolytes or cathode materials delay the onset voltage for oxidation and gassing in coin cells. Note however that the cell impedance is inversely related with battery dimensions. This means that once the same formulation or approach is implemented in realistic batteries, the onset voltages of side reactions will occur earlier than



Pursuant to the DOE Public Access Plan, this document represents the authors' peer-reviewed, accepted manuscript.
The published version of the article is available from the relevant publisher.

what has been observed in coin cells. In general, for a given electrolyte, larger cell formats require earlier onset voltages to control for gassing.

**Fundamental relationship between electrical double layer (EDL) and interphase layer formation:** Electrochemically, the CEI (or SEI) formation processes are closely related to the components within the EDLs[32] developed in the vicinity of the electrode before any electrochemical or side reactions start **(**Fig. 3). Before charge transfer happens, anions adsorb on the positively charged cathode materials surface (left side in Fig.3) along with a small number of solvent molecules, forming an inner Helmholtz layer (IHL). As the positively charged surface continues to be polarized, these anions will be oxidized and converted to the CEI components. Solvent molecules within the IHL will also be oxidized, but unless they have a strong adsorption capability to the positive electrode or possess a very low energy-barrier for oxidation, anions will always be initially oxidized within IHL. Therefore, to tune the composition and properties of CEI layers, the addition of certain anions that will be preferentially oxidized during charging to form an enhanced inorganic layer for CEI may be valuable. If certain solvent additives that are known to help enhance CEI properties are used in the electrolyte, they need to have a strong adsorption ability on the positively charged electrode to fully unlock their potentials to enhance CEI properties.

The relationship between the IHL and the passivation film formation process provides avenues to rationalize why concentrated electrolytes can be used to manipulate the CEI[34] (and SEI[35]). As the concentration of Li salts increases, anions become more abundant in the IHLs of both positive and negative sides and, therefore, enhance the contribution of anion-derived inorganic components in the passive films formed on the electrodes. Note that the formation of the CEI (and SEI) depend on the Gibbs free energy difference between the reactants (electrolytes) and products after the electrochemical/chemical reactions[33], but some qualitative trends can be established by comparing the energies of the highest occupied molecular orbital (HOMO) and lowest unoccupied molecular orbital (LUMO) of different electrolyte components.

More evidence can be found in Table 3 which summarizes the functional electrolytes and additives that have been reported in the literature for use with Ni-rich cathodes. Here, we only consider the results for Ni-rich cathodes tested in full coin or pouch cells for the reasons we have discussed earlier. When the oxidation of Ni-rich materials intensifies at high potentials, conventional carbonates become thermodynamically unstable on their surfaces[36]. EC plays a vital role in forming a stable SEI on graphite, but it undergoes significant decomposition concurrently at the cathode side and generates $CO_2$, CO, and $H_2O$. These reactions are further aggravated in the presence of active oxygen released from Ni-rich NMC at elevated potentials[37]. EC-free electrolytes have been proposed to enhance the anodic stability on Ni-rich cathodes by incorporating multiple Li salts in linear carbonates[38], which in fact tunes the anions within the cathode IHL. Solvents with great stability, such as sulfones[39], sulfonates[40], nitriles[41], fluorinated carbonates and ethers[3,42-49] are also proposed to enhance CEI properties. However, it is important to remark that the change of solvent molecules in the electrolyte can preferentially impact the SEI since solvents are the dominant species in the IHL of negative electrode (Fig. 3). Therefore, any evaluation of solvent modification to enhance the CEI must eventually contend with evaluations of whether the quality of the SEI is, at least, not degraded, which demands further dedicated investigations. Decoupling the cathode and anode reactions is critical to understand which component is being impacted more significantly when even a small change is introduced to the cell[50].



Pursuant to the DOE Public Access Plan, this document represents the authors' peer-reviewed, accepted manuscript.
The published version of the article is available from the relevant publisher.

To replace conventional EC-based electrolytes for Li-ion batteries, an overall assessment on the large full cell performances including cycling stability, rate capability, low/high-temperature performance, shelf life, and resistance to abuse, is necessary. At this moment, additives in the form of either solvents or anions, rather than completely switching to a non-carbonate solvent, probably offer more viable pathways for practical applications. Additives that can kinetically form a robust CEI layer on the cathode and prevent further electrolyte decomposition at high voltages are also reported. Many of these additives such as carbon[51], phosphorus[52], boron[53], sulfur[54], and nitrogen[55] based compounds, or their combinations[56,57] have been developed for cathode materials with relatively low Ni (Ni < 0.8) content, e.g., NMC442[58,59] or NMC532[60,61], but operating at voltages of ≥ 4.4 V (vs. graphite). More full cell work is needed to confirm the effectiveness of these previously explored additives for Ni-rich NMC (Ni ≥ 0.8) charged up to 4.4 V (vs. graphite).

While different electrolyte recipes should be developed depending on the specific applications of Li-ion batteries, the unstable nature of Ni-rich surfaces is the root cause that has delayed the large-scale commercialization of high Ni-content NMC, and therefore needs to be addressed first. In addition to the electrolyte itself, appropriate selection of doping elements or artificial coating layers on cathode may also help to mitigate the electrolyte decomposition and gassing issues commonly found for Ni-rich cathodes.

## Integrate characterization and modeling tools to revisit the CEI

### Characterizing the CEI without ambiguity

Since the discovery of the existence of CEI layers on cathodes in the 1980s[62], there have been many advances in investigating the chemical composition, microstructure, and electronic structure for Li-ion batteries and beyond.

To achieve a holistic understanding of the CEI without ambiguity, there is a critical need to develop advanced characterization techniques that are non-destructive, in-situ/operando and that have high sensitivity, lateral/spatial/temporal resolution, throughput, and automation attributes, and further combine with advanced multiscale modeling tools as shown in Figure 4. Tool selection also need to address the challenges associated with directly probing the dynamically evolving structure, chemistry, and properties of CEI. These challenges arise not only from the different chemical nature and operating conditions, but also from less controllable factors such as preparation route, porosity, and surface morphology/impurities of the cathode architecture. For example, the surface native film (LiOH, $Li_2CO_3$) formed on a NMC cathode during synthesis, storage and assembly add significant complications to CEI formation and characterization. Model cathode materials with controllable surface properties are critical for CEI investigations with definitive results. Flooding of electrolytes will also introduce more interactions between electrolyte, carbon black, and binder as well as unlock possible pathways of CEI redissolution, adding a vast permutation of parameters that impede the isolation of key mechanisms underpinning the reactivity of the electrolyte and cathode material at their interfaces[63,64].

First, due to the sensitive and fragile nature of the CEI, passive and highly sensitive characterization is required to capture its native microstructure and chemistry with minimal damage. For example, TEM could provide atomic scale microstructure and chemical information simultaneously, but the high energy of the electron beam and sample preparation via ion milling



Pursuant to the DOE Public Access Plan, this document represents the authors' peer-reviewed, accepted manuscript.
The published version of the article is available from the relevant publisher.

or ultramicrotomy will compromise the integrity of the CEI. Beam damage can also occur with synchrotron techniques, such as surface sensitive soft X-rays. Recent advancements in cryogenic TEM with direct electron detectors and by using nanosized particles, can help to reduce some of the damage routes of the CEI[65].

Second, combining techniques that are spatially, laterally or temporally resolved is essential to obtain a more reliable and comprehensive understanding of the CEI. Surface sensitive techniques, such as X-ray photoelectron spectroscopy (XPS), time-of-flight secondary ion mass spectroscopy (TOF-SIMS), soft X-ray absorption spectroscopy (sXAS) and related techniques, have been used to elucidate the chemical distribution of large areas within the CEI. Yet they lack sufficient spatial resolution to resolve the nano structural species that may develop as a function of exact lateral location on the surface. TEM could resolve nanoscopic heterogeneity of the CEI, but the size of the field of view that can be measured in reasonable experimental times raises the perennial question of how representative the observations could be[62,66,67]. This gap could be closed with the use of Atomic Force Microscopy (AFM) to gain global information on the surface properties of materials or electrodes by rastering large areas with high nanoscale resolution.

Third, real time monitoring of the CEI dynamic evolution (morphology, composition, and fine structure) is critical to understand its role on the electrochemical performance of a battery[68]. As discussed above, in situ/operando experiments should be meticulously designed, benchmarked and optimized. Depending on the specific technique, the in situ set up may not deliver similar electrochemical performance (i.e., capacity) to that from the real cells. However, it should be ensured that the key electrochemical features (oxidation/reduction peaks) are observed so that the information obtained accurately reflects in situ/operando conditions and remains relevant with practical cells.

Fourth, in addition to imaging-based and spectral-based techniques, measurement and in-situ monitoring of the properties associated with CEI evolution, e.g., ionic conductivity, electrical conductivity, mechanical and thermal response are also important to unravel the relationship between CEI components and macroscopic cell behavior. For example, in situ biasing in TEM was recently applied to measure the electronic conductivity of SEI, and correlated it to SEI composition and eventually the electrolyte chemistry[69]. Scanning electrochemical microscopy (SECM), which can give topological information as well as map conductivities over a large area, provides another opportunity to correlate CEI component and properties, and eventually the battery performance. While exciting, a critical set of next steps should involve a careful evaluation of the design of the experiment so that the conditions that are analyzed approach those in a device, to build real correlations between CEI and cell performance.

Fifth, current understanding and characterization of the CEI mainly focuses on cells at the lab scale (i.e., coin cells). Moving forward, we suggest charting paths to scale up this understanding to 18650 cylindrical or pouch cells, and eventually the pack level under realistic cycling conditions, which will bring the most impactful benefit to industry[70]. Traditional surface analysis techniques are often unable to directly access these buried interfaces due to their inaccessible location within the cell. Consequently, developing innovative methods for in situ or operando characterization becomes essential to gain insights into the behavior and properties of these buried surfaces during cell operation. Fiber/sensor-based devices integrated to such large format cells could be an



Pursuant to the DOE Public Access Plan, this document represents the authors' peer-reviewed, accepted manuscript.
The published version of the article is available from the relevant publisher.

effective method to monitor chemical, thermal, and molecular level evolution of battery components[71].

Last, in situ/operando experiments generate huge image and spectral datasets. Properly processing and analyzing data becomes time-consuming tasks, which can also introduce artifacts. Combining machine learning (ML), artificial intelligence (AI), and advanced characterization techniques could accelerate the data acquisition and analysis in a way that is less labor intensive, reduces human error, while maximizing throughput, and automation, which will bring new opportunities for unprecedented progress to solve the pressing challenges in CEI characterization.

Nevertheless, providing unbiased interpretations of such experimental results can be nontrivial. For example, many chemical species or local structural motifs that emerge in the CEI present characteristic signals that may differ from those in the bulk. However, this signal disparity may be sufficient to preclude easily detecting them within experiment measurements, which provide a non-local ensemble averaged measurement of the interface. It is also difficult to elucidate the unique contributions of a given species to the CEI formation and function during operation, especially if they are short-lived and fail to be captured by any experimental probes. In this regard, integrating experimental characterization techniques with complementary modeling and simulations at the atomic scale will be highly rewarding as it will help to establish a comprehensive understanding of CEI formation and function as shown in Fig. 4.

## Challenges and Opportunities in Simulating CEI

Classical molecular dynamics (MD) simulations based on empirical representations of interatomic interactions are routinely used to probe interfacial structures and resolve populations of key chemical constituents of the interface[73-75]. Although this approach may still be time-limited, coupling classical methods with enhanced sampling techniques can enable a more efficient exploration of potential energy surfaces for out-of-equilibrium reactions and processes[76-78]. The major drawbacks of this approach are the accuracy and transferability of empirical interatomic potentials due to the lack of electronic representation of chemical interactions; these limitations are apparent for even well-parameterized potentials or the more sophisticated class of reactive force fields. To overcome these challenges, force fields based on modern ML that can preserve quantum-level accuracy but at a fraction of the computational cost become increasingly attractive. With the predictive power of MD simulations coupled with high-fidelity ML models, it is now possible to survey a wide range of interfacial atomic arrangements and associated reaction pathways and it is becoming increasingly feasible to track interfacial evolution under relevant experimental conditions[73,74,79,80].

A potential caveat of directly applying atomistic-scale simulations to study CEI is that any resulting prediction derived from these simulations will exhibit a strong dependence on the quality and complexity of the underlying atomic models. Although this practice presents an opportunity to help isolate and to explore individual factors that contribute to the formation and evolution of the CEI and thus allow the elucidation of structure-property relationships at the interface, it lacks the critical emphasis of realism. Specifically, within this framework, it remains challenging to understand the relevance of key structural and chemical features captured in the model in relation to the materials being used in real electrochemical devices.



Pursuant to the DOE Public Access Plan, this document represents the authors' peer-reviewed, accepted manuscript.
The published version of the article is available from the relevant publisher.

Therefore, it is highly desirable to integrate modeling and simulation with solid experimental results and advanced characterization approaches for cross-validation. This concept is illustrated partly in Fig. 4. Upon materials selection, baseline measurements can be conducted to inform modeling factors, such as composition, exposed crystallographic facets of the cathode, local charge/discharge states, etc., and advise the choice of simulation protocols. Due to the potential complications in modeling open shell transition metal oxides using density functional theory (DFT)[81,82], special care needs to be taken and comprehensive benchmark tests may become necessary for selecting the appropriate level of theory or DFT exchange-correlation functionals. This is not only critically important to accurately describe the electronic interaction of the cathode material with electrolyte components and thus to predict the propensities for interfacial degradation, but it is also essential for providing reliable training datasets for the development of advanced ML models. Once the ML potentials are successfully trained and validated, large-scale MD simulations with enhanced sampling can be performed to survey the complex interfacial structure, identify kinetically competing reaction pathways, and extract key chemical motifs or representative configurations appeared during interfacial evolution or degradation for spectroscopy calculations. These calculated spectroscopy signatures can be directly used to deconvolute the experimental spectra and provide unbiased elucidation of interfacial sensitivity to external stimuli, such as processing and cell cycling conditions[83-85]. The comparison with experiment will provide feedback to refine simulation models if necessary to ensure dominate structural and chemical features of interfaces are fully captured. Based on this well implemented experiment-theory feedback loop, a foundational understanding of CEI formation can be established for the model system built and tested using the aforementioned consistent protocol. Positive or negative impacts brought by additives or coating layers used to modify CEI can be analyzed using the same modeling approach to advise design strategies for manipulating the structure and chemistry of CEI to achieve desired performance.

By comparing the theoretical results with experimental measurements collected for samples prepared using different synthetic methods or treated under different conditions, interfacial models can be iteratively revised to ensure essential structural motifs and key chemistry are fully captured. It is only through a well-implemented and well-executed, tightly coupled experiment-simulation approach that a comprehensive atomic-scale description of the dynamically evolving interface can be obtained and its impact on the device-level performance can be elucidated.

## Conclusions and outlook

Identifying and tackling challenges related to the CEI at scales relevant to industry is crucial for the successful translation of materials innovation from academic research to industrial application. A distinct methodology is necessary to re-examine CEI fundamentals on an industrial scale.

To study CEI effectively, it is imperative to ensure that observed electrochemical performance is predominantly influenced by CEI rather than SEI or other factors. Utilizing a stable anode such as graphite as the counter electrode and testing electrochemical cells under conditions relevant to practical applications are essential. Employing a coin cell protocol with parameters close to those of realistic batteries is critical for bridging the scientific gap between small-scale button cells and practical batteries, facilitating fair result comparison among researchers.



Pursuant to the DOE Public Access Plan, this document represents the authors' peer-reviewed, accepted manuscript.
The published version of the article is available from the relevant publisher.

Using a model cathode material with validated baseline performances obtained through coin cell protocols will effectively benchmark future results after modifying CEI through surface coating, new electrolytes, or additives. It is crucial to select the best-performing baseline, which can be updated and improved over time. Additionally, tuning anions, rather than solvent molecules, may be more effective in tailoring CEI properties, unless specific solvent molecules strongly adsorb on the positive side. More efforts are required to identify compatible electrolytes for high-Ni NMC cathodes, such as NMC90 and beyond, which exhibit instability and only cycle within a narrow electrochemical window due to continuous cathode impedance growth.

Capturing the transient changes in CEI morphology at different time scales and spatial dimensions remains challenging yet highly significant. Overcoming challenges such as reducing beam damage on samples and enhancing the relevance of probed images to practical batteries is essential. Cross-validating observed phenomena using various techniques and testing related hypotheses with proposed coin cell protocols could be a potential approach to quickly confirm or refute conclusions drawn from characterizations. Ideally, non-destructive operando characterization tools are needed to directly observe the rapid evolution of CEI in realistic batteries at different scales.

Modeling and simulating CEI properties begin with understanding those formed in baseline cells and progress to CEI with enhanced properties validated through coin cell protocols. All simulation results based on validated experimental data will be valuable in building a database for the development of advanced machine learning models to predict more effective electrolyte recipes or surface engineering strategies accurately.

**Data Availability:** All relevant data are included in the paper.

**Acknowledgments:** This work was supported by the Assistant Secretary for Energy Efficiency and Renewable Energy, Office of Vehicle Technologies of the U.S. Department of Energy (DOE) through Cathode-Electrolyte Interphase (CEI) Consortium. Pacific Northwest National Laboratory (PNNL) is operated by Battelle for the Department of Energy under contract DE-AC05-76RL01830. Part of work was performed under the auspices of the U.S. DOE by Lawrence Livermore National Laboratory under Contract DEAC52-07NA27344.

**Competing interests:** The authors declare no competing interests.



Pursuant to the DOE Public Access Plan, this document represents the authors' peer-reviewed, accepted manuscript. The published version of the article is available from the relevant publisher.

**Table 1 | Full coin cell parameters in standard testing protocol developed at PNNL.**

| **Cathode: NMC811 (polycrystals or single crystals)** | |
|---|---|
| Active material % | 96 wt% |
| Carbon% | 2 wt% |
| PVDF% | 2 wt% |
| Mass loading (NMC only) | ~15 mg/cm$^2$ |
| Specific capacity | ~200 mAh/g (C/10) |
| Areal Capacity | ~ 3 mAh/cm$^2$ |
| Voltage Window | 2.6-4.3V **vs. Gr** (2.7-4.4 V **vs. Li**) |
| Porosity | ~ 35% |
| **Graphite Anode** | |
| Areal Capacity | 3.6 mAh/cm$^2$ |
| Porosity | 40-45% |
| N/P | ~1.2 |
| Baseline Electrolyte | 1M $LiPF_6$ in EC/EMC(3:7)+2%VC |
| Formation Cycle | C/10 for charge & discharge for 3 cycles |
| Charge | CC-CV: C/3 to 4.3V (vs. Gr) then constant voltage until I≤ C/20 |
| Discharge | C/3 |



Pursuant to the DOE Public Access Plan, this document represents the authors' peer-reviewed, accepted manuscript.
The published version of the article is available from the relevant publisher.

**Table 2 | Usable capacity and energy from NMC811 charged to different voltages in a 100 kWh Li-ion battery pack.**

| Material | Voltage Window (V) | Usable Capacity (mAh/g) | Average Discharge Voltage (V) | Material Energy (Wh/kg) | Total NCM mass in 100 kWh LIB pack (kg) | Co Mass (kg) |
|---|---|---|---|---|---|---|
| NMC811 | 2.7-4.1 | 180 | 3.6 | 648 | 154 | 9.3 |
| | 2.7-4.2 | 190 | 3.65 | 694 | 144 | 8.7 |
| | 2.7-4.3 | 199 | 3.7 | 736 | 136 | 8.2 |
| | 2.7-4.4 | 204 | 3.7 | 759 | 132 | 8.0 |
| **Material** | **Voltage Window (V)** | **Usable Capacity (mAh/g)** | **Average Discharge Voltage (V)** | **Material Energy (Wh/kg)** | **Total NCM mass in 100 kWh LIB pack (kg)** | **Co Mass (kg)** |
| NMC90 | 2.7-4.1 | 185 | 3.69 | 683 | 146 | 4.4 |
| | 2.7-4.2 | 195 | 3.73 | 727 | 137 | 4.2 |
| | 2.7-4.3 | 204 | 3.76 | 767 | 130 | 3.9 |
| | 2.7-4.4 | 212 | 3.78 | 803 | 125 | 3.8 |

* Voltage is vs. graphite; capacity is obtained at C/3 rate.



Pursuant to the DOE Public Access Plan, this document represents the authors' peer-reviewed, accepted manuscript. The published version of the article is available from the relevant publisher.

**Table 3 | Functional electrolytes for NMC811 in coin/pouch type Li-ion batteries using graphite as the anode.**

| Electrolyte Recipes | Battery Type | Working voltage (V vs. Gr) | Cathode Loading or areal capacity ($mg/cm^2$ or $mAh/cm^2$) | Capacity Retention | Charge/ discharge rate | Ref |
|---|---|---|---|---|---|---|
| **Based on solvent change or mixing** | | | | | | |
| $LiPF_6$:MDFA:PFPN:FEC (1:7:0.5:1 by mol) | 240 mAh pouch cell | 2.8-4.3 | 13.2 | 81.8% @ 500 cycles | 1C/1C | 42 |
| 1.0 M $LiPF_6$ PC:TFA (3:7 by vol) | 730 mAh pouch cell | 2.7-4.3 (45 °C) | 12.1 | 82%@400 cycles | 1C/1C | 43 |
| 1.6 M LiFSI TEOSCN | 1 Ah pouch cell | 2.8-4.3 | N/A | 95%@500 cycles | 0.2C/ 0.2C | 41 |
| 1.0 M $LiPF_6$/0.02 M LiDFOB FEC:HFE:FEMC (2:2:6 by vol) | 1 Ah pouch cell | 3-4.3 | N/A (single crystal 811 used) | 110.1%@ 200 cycles | 0.33C/0.3 3C | 42 |
| LiFSI:DMC:EC:TTE (1:4.8:0.2:1 by mol) | Coin cell | 2.5-4.4 | 1.5 $mAh/cm^2$ | 69%@ 300 cycles | 4C/ 0.33C | 3 |
| 1.0 M $LiPF_6$ SL:FEC:EMC (1:1:3 by vol) + 0.5wt % $LiBF_4$/$LiNO_3$ | Coin cell | 2.75-4.4 | 20 | 85.2%@ 300 cycles | 0.5C/ 0.5C | 39 |
| 1.0 M $LiPF_6$ in FEC:TTE (6:4 by vol) | 1 Ah pouch cell | 3-4.4 | N/A | 91%@ 300 cycles | 1C/1C | 45 |
| LiFSI:DME:FEC:PFPN (1:1.5:0.5:3 by mol) | coin cell | 2.5-4.5 | 8.35 | 82%@1000 cycles | 0.33C/0.3 3C | 46 |
| 1.0 M LiTFSI MDFA:MDFSA:TTE (4:1:5 by mol) | Coin cell | 2.5-4.5 | 11.5 | 80.1%@ 400 cycles | 0.5C/ 0.5C | 48 |
| 0.8 M LiFSI-0.1 M LiTFSI-0.6 M $LiPF_6$ EMC | 1 Ah pouch cell | 3-4.5 | 13.5 | 82.1%@ 200 cycles | 0.33C/ 0.33C | 38 |
| 1.9 M LiFSI TTMS:TM (1:2 by vol) | 1 Ah pouch cell | 3-4.6 | N/A | 83%@1000 cycles | 0.5C/ 1C | 40 |
| LiDFOB:MP:mFT:TTE (1:2.67:1:1 by mol) | 1.2 Ah pouch cell | 2.8-4.6 | 17.4 | 90.4%@ 130 cycles | 0.2C/ 0.2C | 47 |
| **Based on anion change or mixing** | | | | | | |
| 1.0 M $LiPF_6$ EC:EMC (3:7 by wt) + 0.4wt% $NaH_2PO_4$ | Coin cell | 3-4.3 (60 °C) | 2.6 $mAh/cm^2$ | 150 cycles @ 75%, 0.5C/0.5C | | 52 |
| 1.0 M $LiPF_6$ EC:EMC (3:7 by vol) + 2wt% VC | 200 mAh pouch cell | 2.8-4.4 (40 °C) | N/A | 200 cycles @ 80%, 0.2C/0.2C | | 51 |
| 1.0 M $LiPF_6$ EC:EMC (3:7 by vol) + 2wt% VC + 2wt% LiDFOB + 1wt% TMSPi | Coin cell | 2.5-4.5 | 24 | 300 cycles @ 85%, 0.2C/0.5C | | 56 |
| 1.0 M $LiPF_6$ EC:DEC (1:1 by vol) + 2wt% TMSP+ 0.1 M LiDFOB | Single layer pouch cell | 2.7-4.5 | N/A | 500 cycles @ 82.8%, 1C/1C | | 57 |
| 1.0 M $LiPF_6$ EC:EMC (1:2 by vol) + 1wt% DES | 1.95 Ah pouch cell | 2.75-4.5 | N/A | 150 cycles @ 82.5%, 1C/1C | | 54 |

Abbreviation:



Pursuant to the DOE Public Access Plan, this document represents the authors' peer-reviewed, accepted manuscript. The published version of the article is available from the relevant publisher.

Methyl difluoroacetate (MDFA); Ethoxy-pentafluoro-cyclotriphosphazene (PFPN); Fluoroethylene carbonate (FEC); Propylene carbonate (PC); 2,2,2-trifluoroethyl acetate (TFA); (2-cyanoethyl)triethoxysilane (TEOSCN); (2,2,2-trifluoroethyl) carbonate (FEMC); Dimethyl carbonate (DMC); Ethylene carbonate (EC); 1,1,2,2-tetrafluoroethyl-2,2,3,3-tetrafluoropropyl ether (TTE); Sulfolane (SL); Ethyl methyl carbonate (EMC); Ethoxy(pentafluoro) cyclotriphosphazene (PFPN); Dimethoxyethane (DME); Methyl difluoroacetate (MDFA); Methyl 2,2-difluoro-2 (fluorosulfonyl)acetate (MDFSA); 2,2,2-trifluoroethyl trifluoromethanesulfonate (TTMS); 2,2,2-trifluoroethyl methanesulfonate (TM); Methyl propionate (MP); m-fluorotoluene (mFT); Vinylene carbonate (VC); Tris(trimethylsilyl)phosphite (TMSPi); Diethyl carbonate (DEC); Tris(trimethylsilyl)phosphate(TMSP); 3,3-Diethylene Di-Sulfite (DES); 2,2,7,7-tetramethyl-3,6-dioxa-2,7-disilaoctane-4,4,5,5-tetracarbonitrile (TDSTCN).



Pursuant to the DOE Public Access Plan, this document represents the authors' peer-reviewed, accepted manuscript.
The published version of the article is available from the relevant publisher.

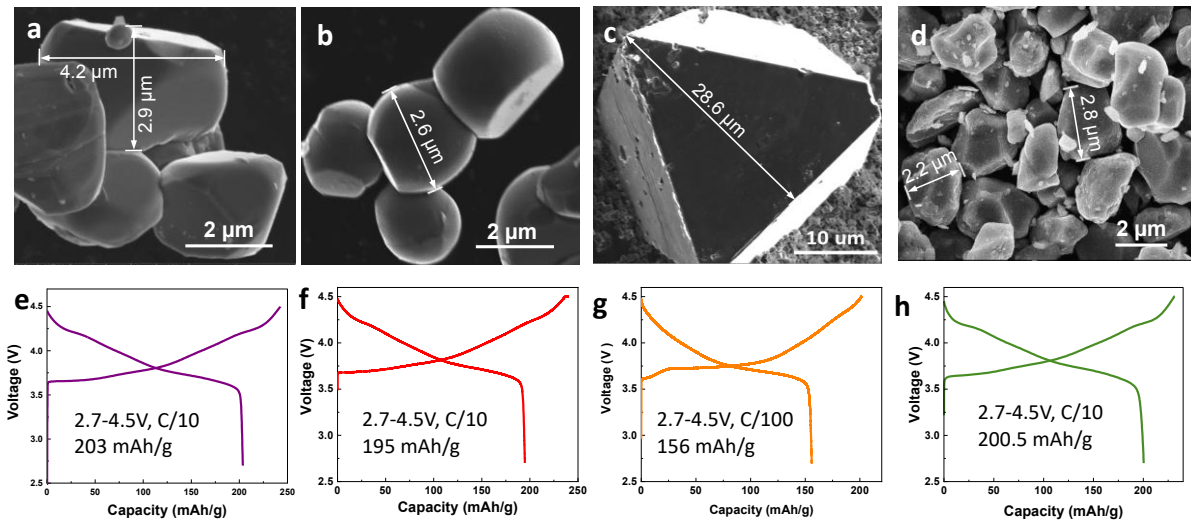


**Fig. 1** | Single crystal Ni-rich NMC with different morphologies as model materials. **a**, single crystal NMC76 with an average crystal size of 3-4 μm. **b**, modified single crystal NMC76 with drum-like morphologies. **c**, ca. 30 μm large single crystal NMC76 with (001) and (012) planes exposed, ideal for in situ characterizations. **d**, Single crystal NMC811 with irregular morphologies. **e**, The charge-discharge curve of single crystal NMC76 in **a**. 203 mAh/g capacity is delivered when charged to 4.5 V vs. $Li/Li^+$. **f**, The charge-discharge curve of drum-like single crystals in **b**. 195 mAh/g capacity is delivered when charged to 4.5 V vs. $Li/Li^+$. **g**, The charge-discharge curve of 20 μm single crystal in **c**. At a very slow rate of C/100, still 156 mAh/g capacity is delivered from such as huge crystal when charged to 4.5 V vs. $Li/Li^+$. **h**, The charge-discharge curve of ca. 2 μm single crystal in **d**. 202 mAh/g capacity is obtained when charged to 4.5 V vs. $Li/Li^+$. **a-c** are synthesized by a molten salt approach[13], while **d** is prepared by solid state synthesis[72].



Pursuant to the DOE Public Access Plan, this document represents the authors' peer-reviewed, accepted manuscript.
The published version of the article is available from the relevant publisher.

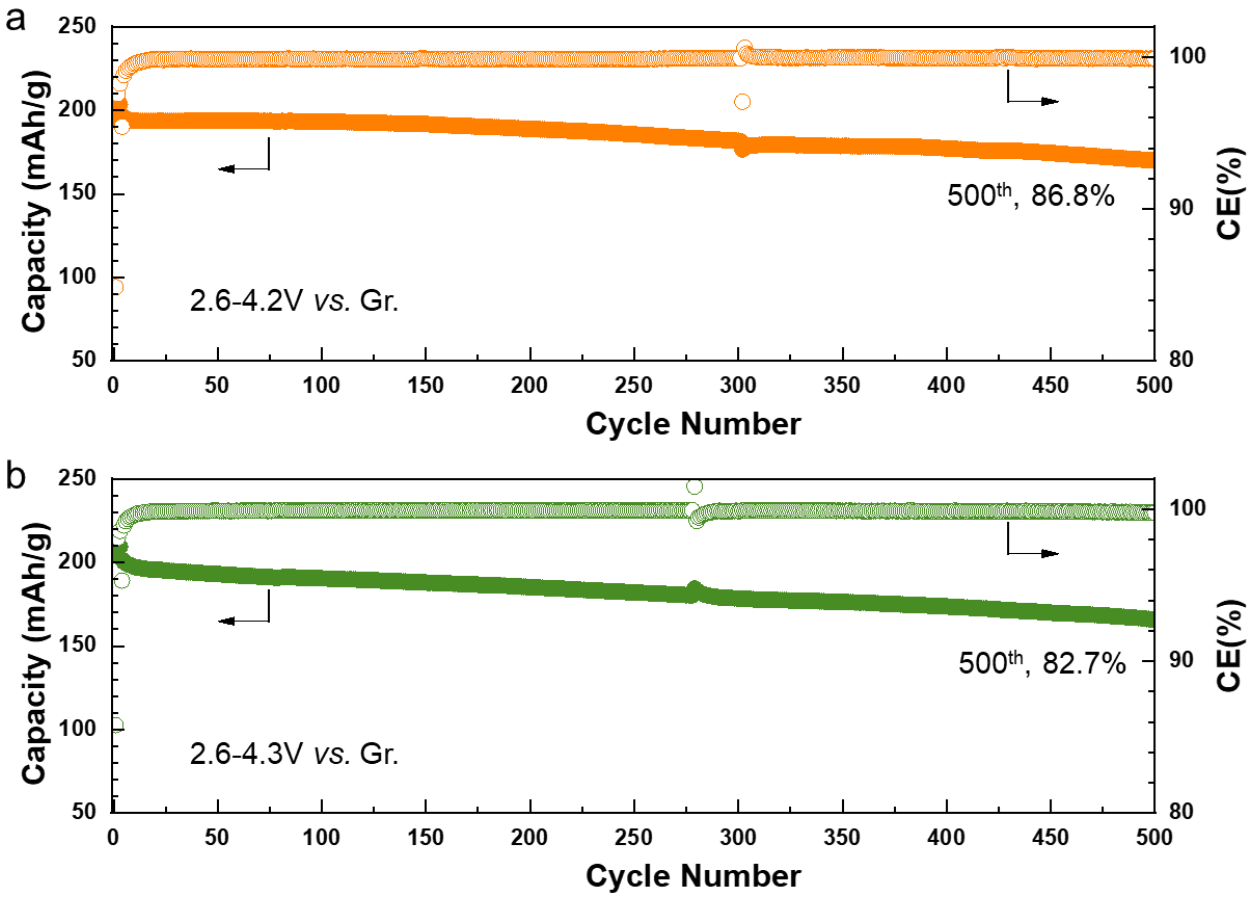


**Fig. 2** | Electrochemical performances of NMC811 polycrystals tested in full coin cells which use graphite as anode. **a**, Cycling performance of NMC811 tested between 2.6-4.2 V vs. Gr. **b**, Cycling performance of NMC811 tested between 2.6-4.3 V vs. Gr. Commercial NMC811 cathode and graphite anode materials are used in this full coin cell testing by using the protocols listed in Table 1. Baseline electrolyte. i.e., 1M $LiPF_6$ in EC/EMC+2%VC, is used for coin cell testing. C/3 was used for both charge and discharge after three formation cycles at C/10. 1C was named as 200 mA/g. These performances can be used as baseline performances to benchmark any further modification on cathode, anode or electrolyte etc.



Pursuant to the DOE Public Access Plan, this document represents the authors' peer-reviewed, accepted manuscript.
The published version of the article is available from the relevant publisher.

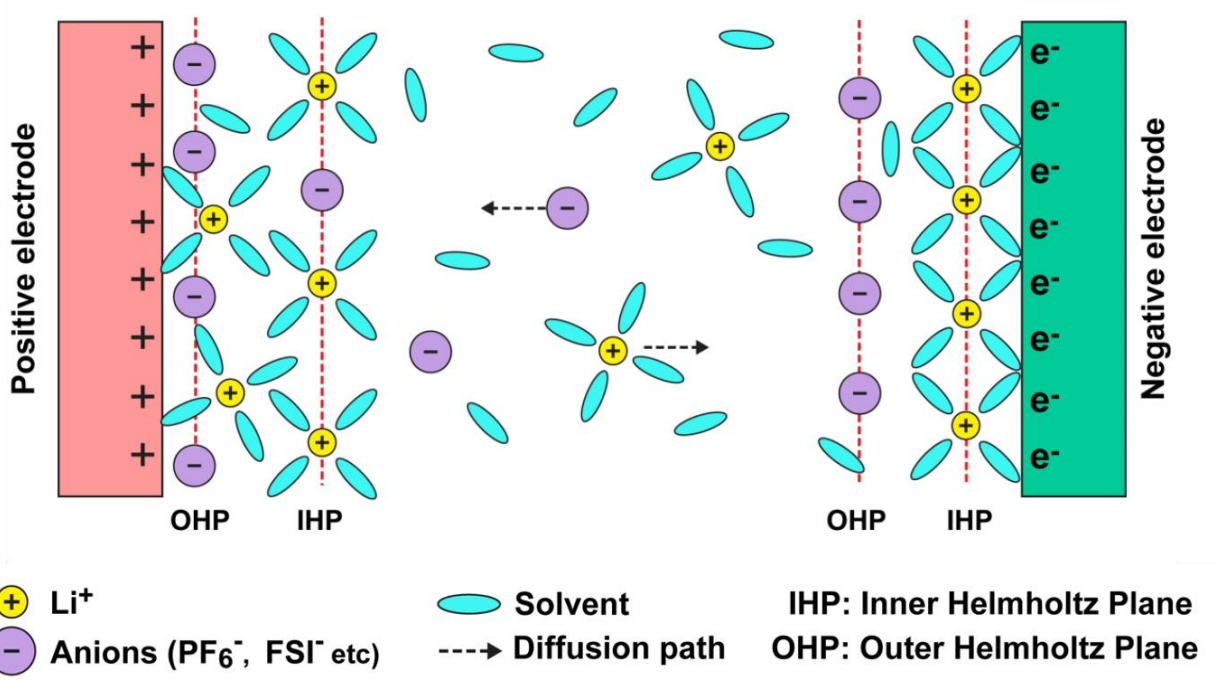


545

546 **Fig. 3 | Electrical double layers formed on positive electrode and negative electrode sides**
547 **during charge process.** The constituents in the inner Helmholtz layer are related to the later
548 formed passion layers on positive and negative electrodes, which can be used to help develop better
549 electrolytes or additives to tune CEI or SEI properties.

550

551



Pursuant to the DOE Public Access Plan, this document represents the authors' peer-reviewed, accepted manuscript.
The published version of the article is available from the relevant publisher.

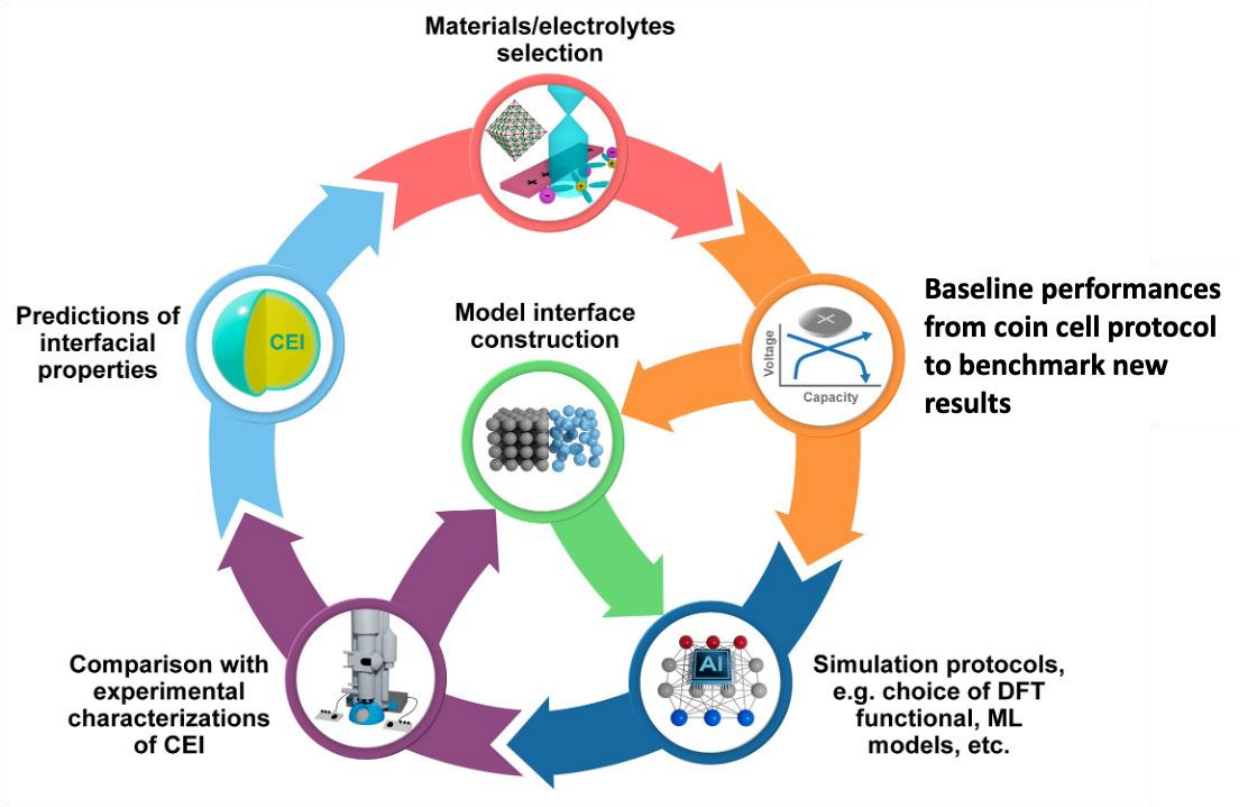


552

553 **Fig. 4 | An approach for resolving the chemical and structural features of complex**
554 **electrochemical interfaces based on the integration of experiments and theory.** Libraries of
555 local interfacial structures and their associated chemical and structural signatures are constructed
556 and compared against experimentally-measured signatures in order to iteratively refine structural
557 and chemical models.

558

559

560



Pursuant to the DOE Public Access Plan, this document represents the authors' peer-reviewed, accepted manuscript.
The published version of the article is available from the relevant publisher.

# References


1 Xu, K. Electrolytes and interphases in Li-ion batteries and beyond. *Chem. Rev.* **114**, 11503-11618 (2014).

2 Ohzuku, T., Iwakoshi, Y. & Sawai, K. Formation of lithium-graphite intercalation compounds in nonaqueous electrolytes and their application as a negative electrode for a lithium ion (shuttlecock) cell. *J. Electrochem. Soc.* **140**, 2490 (1993).

3 Kautz, D. J. et al. Designing electrolytes with controlled solvation structure for fast-charging lithium-ion batteries. *Adv. Energy Mater.* **13**, 2301199 (2023).

4 Zhang, X. et al. Advanced electrolytes for fast-charging high-voltage lithium-ion batteries in wide-temperature range. *Adv. Energy Mater.* **10**, 2000368 (2020).

5 Wen, B. et al. Ultrafast ion transport at a cathode–electrolyte interface and its strong dependence on salt solvation. *Nat. Energy* **5**, 578-586 (2020). **A study that reveals the relationship between desolvation energy and CEI's interfacial kinetics.**

6 Björklund, E. et al. Cycle-induced interfacial degradation and transition-metal cross-over in $LiNi_{0.8}Mn_{0.1}Co_{0.1}O_2$–graphite cells. *Chem. Mater.* **34**, 2034-2048 (2022).

7 Liu, W. et al. Inhibition of transition metals dissolution in cobalt-free cathode with ultrathin robust interphase in concentrated electrolyte. *Nat. Commun.* **11**, 3629 (2020).

8 Gutierrez, A. et al. Review—Earth-abundant, Mn-rich cathodes for vehicle applications and beyond: Overview of critical barriers. *J. Electrochem. Soc.* **170**, 030509 (2023).

9 Clément, R. J., Lun, Z. & Ceder, G. Cation-disordered rocksalt transition metal oxides and oxyfluorides for high energy lithium-ion cathodes. *Energy Environ. Sci.* **13**, 345-373 (2020).

10 Nelson, K. J. et al. Studies of the effect of high voltage on the impedance and cycling performance of $Li[Ni_{0.4}Mn_{0.4}Co_{0.2}]O_2$/graphite lithium-ion pouch cells. *J. Electrochem. Soc.* **162**, A1046-A1054 (2015).

11 Yan, P. et al. Tailoring grain boundary structures and chemistry of Ni-rich layered cathodes for enhanced cycle stability of lithium-ion batteries. *Nat. Energy* **3**, 600-605 (2018).

12 Hu, J. et al. Locking oxygen in lattice: A quantifiable comparison of gas generation in polycrystalline and single crystal Ni-rich cathodes. *Energy Storage Mater.* **47**, 195-202 (2022).

13 Bi, Y. et al. Reversible planar gliding and microcracking in a single-crystalline Ni-rich cathode. *Science* **370**, 1313-1317 (2020). **A study about how to make a single-crystal, nickel-rich cathode hardier and more efficient.**

14 Lin, F. et al. Metal segregation in hierarchically structured cathode materials for high-energy lithium batteries. *Nat. Energy* **1**, 15004 (2016).

15 Yan, P. et al. Ni and Co segregations on selective surface facets and rational design of layered lithium transition-metal oxide cathodes. *Adv. Energy Mater.* **6**, 1502455 (2016).

16 Zhang, J. et al. Interfacial design for a 4.6 V high-voltage single-crystalline $LiCoO_2$ cathode. *Adv. Mater.* **34**, 2108353 (2022).

17 Choi, S. H., Son, J.-W., Yoon, Y. S. & Kim, J. Particle size effects on temperature-dependent performance of $LiCoO_2$ in lithium batteries. *J. Power Sources* **158**, 1419-1424 (2006).

18 Zhang, X. et al. Electrolyte regulating toward stabilization of cobalt-free ultrahigh-nickel layered oxide cathode in lithium-ion batteries. *ACS Energy Lett.* **6**, 1324-1332 (2021).

19 Jung, R. et al. Effect of ambient storage on the degradation of ni-rich positive electrode materials (NMC811) for Li-ion batteries. *J. Electrochem. Soc.* **165**, A132-A141 (2018).

20 Liu, D. et al. Review of recent development of in situ/operando characterization techniques for lithium battery research. *Adv. Mater.* **31**, 1806620 (2019).




Pursuant to the DOE Public Access Plan, this document represents the authors' peer-reviewed, accepted manuscript. The published version of the article is available from the relevant publisher.

21 Borkiewicz, O. J., Wiaderek, K. M., Chupas, P. J. & Chapman, K. W. Best practices for operando battery experiments: influences of X-ray experiment design on observed electrochemical reactivity. *J. Phys. Chem. Lett.* **6**, 2081–2085 (2015).

22 Chen, S. et al. Critical parameters for evaluating coin cells and pouch cells of rechargeable Li-metal batteries. *Joule* **3**, 1094-1105 (2019). **A study that proposed the coin-cell and pouch-cell critical parameters and testing conditions for the battery research community to bridge the gap between fundamental research and practical adoption of new ideas or materials and to expedite their full integration into realistic battery systems.**

23 Xiao, J. et al. Perspective—Electrochemistry in understanding and designing electrochemical energy storage systems. *J. Electrochem. Soc.* **169**, 010524 (2022).

24 Hu, J. et al. Achieving highly reproducible results in graphite-based Li-ion full coin cells. *Joule* **5**, 1011-1015 (2021).

25 Bi, Y. et al. Highly stable Ni-rich layered oxide cathode enabled by a thick protective layer with bio-tissue structure. *Energy Storage Mater.* **24**, 291-296 (2020).

26 Lu, D. et al. Enabling high-energy-density cathode for lithium–sulfur batteries. *ACS Appl. Mater. Interfaces* **10**, 23094-23102 (2018).

27 Xiao, J. Understanding the lithium sulfur battery system at relevant scales. *Adv. Energy Mater.* **5**, 1501102 (2015).

28 Chouchane, M., Yao, W., Cronk, A., Zhang, M. & Meng, Y. S. Improved rate capability for dry thick electrodes through finite elements method and machine learning coupling. *ACS Energy Lett.* 1480-1486 (2024).

29 Zhang, N. et al. Long-term cycling and mechanisms of cell degradation of single crystal $LiNi_{0.95}Mn_{0.04}Co_{0.01}O_2$/graphite cells. *J. Electrochem. Soc.* **171**, 010520 (2024).

30 Bi, Y., Li, Q., Yi, R. & Xiao, J. To pave the way for large-scale electrode processing of moisture-sensitive Ni-rich cathodes. *J. Electrochem. Soc.* **169**, 020521 (2022).

31 Cao, X. Important factors for the reliable and reproducible preparation of non-aqueous electrolyte solutions for lithium batteries. *Commun. Mater.* **4**, 10 (2023).

32 Wu, Q., McDowell, M. T. & Qi, Y. Effect of the electric double layer (EDL) in multicomponent electrolyte reduction and solid electrolyte interphase (SEI) formation in lithium batteries. *J. Am. Chem. Soc.* **145**, 2473–2484 (2023).

33 Peljo, P. & Girault, H. H. Electrochemical potential window of battery electrolytes: the HOMO–LUMO misconception. *Energy Environ. Sci.* **11**, 2306-2309 (2018).

34 Cao, X. et al. Optimization of fluorinated orthoformate based electrolytes for practical high-voltage lithium metal batteries. *Energy Storage Mater.* **34**, 76-84 (2021).

35 Yamada, Y. et al. Unusual stability of acetonitrile-based superconcentrated electrolytes for fast-charging lithium-ion batteries. *J. Am. Chem. Soc.* **136**, 5039-5046 (2014).

36 Dong, T. et al. Electrolyte engineering toward high performance high nickel ($Ni \geq 80\%$) lithium-ion batteries. *Adv. Sci.* **11**, 2305753 (2023).

37 Rinkel, B. L. D., Vivek, J. P., Garcia-Araez, N. & Grey, C. P. Two electrolyte decomposition pathways at nickel-rich cathode surfaces in lithium-ion batteries. *Energy Environ. Sci.* **15**, 3416-3438 (2022).

38 Wu, Y. et al. High-voltage and high-safety practical lithium batteries with ethylene carbonate-free electrolyte. *Adv. Energy Mater.* **11**, 2102299 (2021).

39 Dai, P. et al. Synergistic effect of dual-anion additives promotes the fast dynamics and high-voltage performance of Ni-rich lithium-ion batteries by regulating the electrode/electrolyte interface. *ACS Applied Mater. Interfaces* **14**, 39927-39938 (2022).




Pursuant to the DOE Public Access Plan, this document represents the authors' peer-reviewed, accepted manuscript. The published version of the article is available from the relevant publisher.

40 Zhang, J. et al. Multifunctional solvent molecule design enables high-voltage Li-ion batteries. *Nat. Commun.* **14**, 2211 (2023).
41 Lu, D. et al. A self-purifying electrolyte enables high energy Li ion batteries. *Energy Environ. Sci.* **15**, 3331-3342 (2022).
42 Zou, Y. et al. Non-flammable electrolyte enables high-voltage and wide-temperature lithium-ion batteries with fast charging. *Angew. Chem. Int. Ed.* **62**, e202216189 (2023).
43 An, K., Tran, Y. H. T., Kwak, S., Han, J. & Song, S.-W. Design of fire-resistant liquid electrolyte formulation for safe and long-cycled lithium-ion batteries. *Adv. Funct. Mater.* **31**, 2106102 (2021).
44 Wu, C. et al. Thermal runaway suppression of high-energy lithium-ion batteries by designing the stable interphase. *J. Electrochem. Soc.* **168**, 090563 (2021).
45 Hou, J. et al. Thermal runaway of lithium-ion batteries employing flame-retardant fluorinated electrolytes. *Energy Environ. Mater.* **6**, e12297 (2023).
46 Chen, L. et al. High-safety and high-efficiency electrolyte design for 4.6 V-class lithium-ion batteries with a non-solvating flame-retardant. *Chem. Sci.* **14**, 1184-1193 (2023).
47 Fang, M. et al. An electrolyte with less space-occupying diluent at cathode inner helmholtz plane for stable 4.6 V lithium-ion batteries. *Angew. Chem. Int. Ed.* **63**, e202316839 (2023).
48 Xu, J. et al. Electrolyte design for Li-ion batteries under extreme operating conditions. *Nature* **614**, (2023). **A work that reports an electrolyte design principle to form stable SEI/CEI for high-energy batteries operating under extreme conditions.**
49 Jia, H. et al. Toward the practical use of cobalt-free lithium-ion batteries by an advanced ether-based electrolyte. *ACS Appl. Mater. Interfaces* **13**, 44339-44347 (2021).
50 Páez Fajardo, G. J. et al. Synergistic degradation mechanism in single crystal Ni-rich NMC//graphite cells. *ACS Energy Lett.* **8**, 5025-5031 (2023).
51 Li, J., Downie, L. E., Ma, L., Qiu, W. & Dahn, J. R. Study of the failure mechanisms of $LiNi_{0.8}Mn_{0.1}Co_{0.1}O_2$ cathode material for lithium ion batteries. *J. Electrochem. Soc.* **162**, A1401-A1408 (2015).
52 Jo, M., Park, S.-H. & Lee, H. $NaH_2PO_4$ as an electrolyte additive for enhanced thermal stability of $LiNi_{0.8}Co_{0.1}Mn_{0.1}O_2$/graphite batteries. *J. Electrochem. Soc.* **167**, 130502 (2020).
53 Li, J., Li, W., You, Y. & Manthiram, A. Extending the service life of high-Ni layered oxides by tuning the electrode–electrolyte interphase. *Adv. Energy Mater.* **8**, 1801957 (2018).
54 Li, S. et al. 3,3-diethylene di-sulfite (DES) as a high-voltage electrolyte additive for 4.5 V $LiNi_{0.8}Co_{0.1}Mn_{0.1}O_2$/graphite batteries with enhanced performances. *ChemElectroChem* **8**, 745-754 (2021).
55 Ren, Z. et al. Delicately designed cyano-siloxane as multifunctional additive enabling high voltage $LiNi_{0.9}Co_{0.05}Mn_{0.05}O_2$/graphite full cell with long cycle life at 50 °C. *Adv. Funct. Mater.* **33**, 2302411 (2023).
56 Zhao, W. et al. Extending the high-voltage operation of graphite/NCM811 cells by constructing a robust electrode/electrolyte interphase layer. *Mater. Today Energy* **34**, 101301 (2023).
57 Cheng, F. et al. Tailoring electrolyte enables high-voltage Ni-rich NCM cathode against aggressive cathode chemistries for Li-ion batteries. *Sci. Bull.* **67**, 2225-2234 (2022).
58 Ma, L., Xia, J. & Dahn, J. R. Improving the high voltage cycling of $Li[Ni_{0.42}Mn_{0.42}Co_{0.16}]O_2$ (NMC442)/graphite pouch cells using electrolyte additives. *J. Electrochem. Soc.* **161**, A2250-A2254 (2014).



Pursuant to the DOE Public Access Plan, this document represents the authors' peer-reviewed, accepted manuscript.
The published version of the article is available from the relevant publisher.

59 Xia, J. et al. Study of triallyl phosphate as an electrolyte additive for high voltage lithium-ion cells. *J. Power Sources* **295**, 203-211 (2015).
60 Keefe, A. S., Weber, R., Hill, I. G. & Dahn, J. R. Studies of the SEI layers in Li($Ni_{0.5}Mn_{0.3}Co_{0.2}$)$O_2$/artificial graphite cells after formation and after cycling. *J. Electrochem. Soc.* **167**, 120507 (2020).
61 Thompson, L. M. et al. Quantifying changes to the electrolyte and negative electrode in aged NMC532/graphite lithium-ion cells. *J. Electrochem. Soc.* **165**, A2732-A2740 (2018).
62 Thomas, M. G. S. R., Bruce, P. G. & Goodenough, J. B. AC impedance analysis of polycrystalline insertion electrodes - application to $Li_{1-x}CoO_2$. *J. Electrochem. Soc.* **132**, 1521-1528. (1985).
63 Demeaux, J., Caillon-Caravanier, M., Galiano, H., Lemordant, D. & Claude-Montigny, B. LiNiMnO/electrolyte and carbon black/electrolyte high voltage interfaces: To evidence the chemical and electronic contributions of the solvent on the cathode-electrolyte interface formation. *J. Electrochem. Soc.* **159**, A1880-A1890 (2012).
64 Gauthier, M. et al. Electrode-electrolyte interface in li-ion batteries: Current understanding and new insights. *J. Phys. Chem. Lett.* **6**, 4653-4672 (2015).
65 Zhang, Z. W. et al. Cathode-electrolyte interphase in lithium batteries revealed by cryogenic electron microscopy. *Matter* **4**, 302-312 (2021).
66 Huang, W., Wang, H., Boyle, D. T., Li, Y. Z. & Cui, Y. Resolving nanoscopic and mesoscopic heterogeneity of fluorinated species in battery solid-electrolyte interphases by cryogenic electron microscopy. *ACS Energy Lett.* **5**, 1128-1135 (2020).
67 Hestenes, J. C. & Marbella, L. E. Beyond composition: Surface reactivity and structural arrangement of the cathode-electrolyte interphase. *ACS Energy Lett.* **8**, 4572-4596 (2023).
68 Lu, J., Wu, T. P. & Amine, K. State-of-the-art characterization techniques for advanced lithium-ion batteries. *Nat. Energy* **2**, 17011 (2017). **A review that summarizes the application of advanced characterization techniques for lithium-ion batteries.**
69 Xu, Y. et al. Direct in situ measurements of electrical properties of solid–electrolyte interphase on lithium metal anodes. *Nat. Energy* **8**, 1345-1354 (2023).
70 Xiao, J., Shi, F. F., Glossmann, T., Burnett, C. & Liu, Z. From laboratory innovations to materials manufacturing for lithium-based batteries. *Nat. Energy* **8**, 329-339 (2023). **A perspective, which reviews challenges and opportunities in scaling up lithium-based battery materials and components to accelerate future low-cost battery manufacturing.**
71 Huang, J. Q., Boles, S. T. & Tarascon, J. M. Sensing as the key to battery lifetime and sustainability. *Nat. Sustain.* **5**, 194-204 (2022).
72 Bi, Y. et al. Simultaneous single crystal growth and segregation of Ni-rich cathode enabled by nanoscale phase separation for advanced lithium-ion batteries. *Energy Storage Mater.* **62**, 102947 (2023).
73 Yao, N., Chen, X., Fu, Z. & Zhang, Q. Applying classical, ab initio, and machine-learning molecular dynamics simulations to the liquid electrolyte for rechargeable batteries. *Chem. Rev.* **122**, 10970-11021 (2022).
74 Tan, X. et al. Decoding Electrochemical processes of lithium-ion batteries by classical molecular dynamics simulations. *Adv. Energy Mater.* 2400564 (2024).
75 Kim, S., van Duin, A.C.T. & Shenoy, V.B. Effect of electrolytes on the structure and evolution of the solid electrolyte interphase (SEI) in Li-ion batteries: A molecular dynamics study. *J. Power Sources* **196**, 8590-8597 (2011).



Pursuant to the DOE Public Access Plan, this document represents the authors' peer-reviewed, accepted manuscript. The published version of the article is available from the relevant publisher.

76 Alzate-Vargas, L. et al. Insight into SEI Growth in Li-ion batteries using molecular dynamics and accelerated chemical reactions. *J. Phys. Chem. C* **125**, 18588-18596 (2021).
77 Gao, H. et al. Enhanced electrolyte transport and kinetics mitigate graphite exfoliation and Li plating in fast-charging Li-ion batteries. *Adv. Energy Mater.* **13**, 2202906 (2023).
78 Holoubek, J. et al. Predicting the ion desolvation pathway of lithium electrolytes and their dependence on chemistry and temperature. *J. Phys. Chem. Lett.* **13**, 4426-4433 (2022).
79 Diddens, D. et al. Modeling the solid electrolyte interphase: Machine learning as a game changer? *Adv. Mater. Interfaces* **9**, 2101734 (2022). **A review that summarizes recent advances in the integration and application of physics-based modeling and machine learning to the study of solid electrolyte interphases in lithium-ion batteries.**
80 Shao, Y., Knijff, L., Dietrich, F.M., Hermansson, K. & Zhang C. Modelling bulk electrolytes and electrolyte interfaces with atomistic machine learning. *Batter. Supercaps* **4,** 585-595 (2021).
81 Saritas, K., Fadel, E.R., Kozinsky, B. & Grossman, J.C. Charge density and redox potential of $LiNiO_2$ using ab initio diffusion quantum Monte Carlo. *J. Phys. Chem. C* **124**, 5893-5901 (2020).
82 Timrov, I., Aquilante, F., Cococcioni, M. & Marzari, N. Accurate electronic properties and intercalation voltages of olivine-type Li-ion cathode materials from extended Hubbard functionals. *PRX Energy* **1**, 033003 (2022).
83 Sun, W., et al. Coupled experimental–theoretical characterization of a carbon electrode in vanadium redox flow batteries using X-ray absorption spectroscopy. *ACS Appl. Mater. Interfaces* **16**, 8791-8801 (2024). **A study that demonstrates tight experiment-theory integration for resolving the impact of electrode surface chemistry on electrochemical cell performance.**
84 Tamura, T., Kohyama, M. & Ogata, S. Combination of first-principles molecular dynamics and XANES simulations for $LiCoO_2$-electrolyte interfacial reactions in a lithium-ion battery. *Phys. Rev. B* **96**, 035107 (2017).
85 Carlier, D. et al. DFT+U calculations and XAS study: Further confirmation of the presence of $CoO_5$ square-based pyramids with IS-$Co^{3+}$ in Li-overstoichiometric $LiCoO_2$. *J. Phys. Chem. C* **117**, 26493-26500 (2013).



Pursuant to the DOE Public Access Plan, this document represents the authors' peer-reviewed, accepted manuscript. The published version of the article is available from the relevant publisher.